Journal of Colloid and Interface Science 564 (2020) 467–477

Contents lists available at ScienceDirect

Journal of Colloid and Interface Science

journal homepage: www.elsevier.com/locate/jcis

Atomic layer deposition of Al_2O_3 on P2-$Na_{0.5}Mn_{0.5}Co_{0.5}O_2$ as interfacial layer for high power sodium-ion batteries

Hari Vignesh Ramasamy [a], Pravin N. Didwal [b], Soumyadeep Sinha [b], Vanchiappan Aravindan [c], Jaeyeong Heo [b], Chan-Jin Park [b], Yun-Sung Lee [a,*]

[a] Department of Advanced Chemicals and Engineering, Chonnam National University, Gwang-ju 61186, Republic of Korea
[b] Department of Materials Science and Engineering, Chonnam National University, Gwang-ju 61186, Republic of Korea
[c] Department of Chemistry, Indian Institute of Science Education and Research (IISER), Tirupati 517507, India

GRAPHICAL ABSTRACT

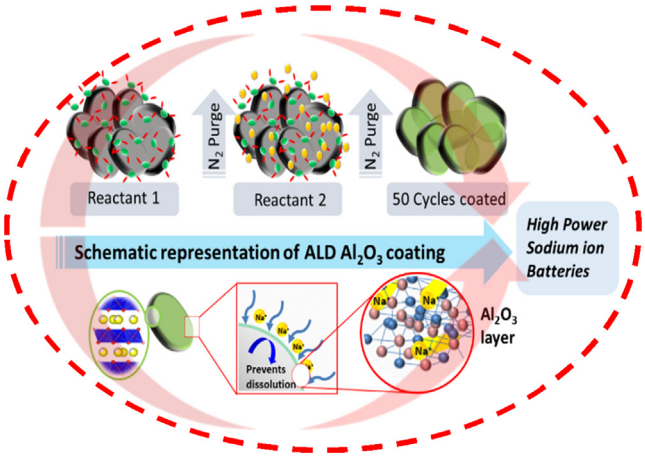

ARTICLE INFO

Article history:
Received 30 August 2019
Revised 26 December 2019
Accepted 31 December 2019
Available online 2 January 2020

Keywords:
Layered oxide
ALD coating
High power
Interfacial engineering
Al_2O_3 coating

ABSTRACT

Surface modification is one of the impressive and widely used technique to improve the electrochemical performance of sodium-ion batteries by modifying the electrode-electrolyte interface. Herein, we used the atomic layer deposition (ALD) to modify the surface of P2-$Na_{0.5}Mn_{0.5}Co_{0.5}O_2$ by sub-monolayer Al_2O_3 coating on the prefabricated electrodes. Phase purity is confirmed using various structural and morphological studies. The pristine electrode delivered an initial discharge capacity of 154 mAh g^{-1} at 0.5C, and inferior rate performance of 23 mAh g^{-1} at 40C rate. On the other hand, the interfacial modified cathode with 5 cycles of ALD coating delivers a high capacity of 174 and 45 mAh g^{-1} at 0.5C and 40C rate, respectively. The $Co^{2+/3+}$ redox couple is utilized for the faradaic process with high reversibility along with suppressed P2-O2 phase transition. The presence of the Al_2O_3 layer acts as an artificial cathode electrolyte interface by suppressing the electrolyte oxidation at higher cutoff potentials. This is clearly validated by the reduced charge transfer resistance of surface modified electrodes after cycling at various current rates. Even at an elevated temperature condition (50 °C), interfacial layer significantly improves the safety of the cell and ensures the stability of the cathode.

* Corresponding author.
E-mail address: leeys@chonnam.ac.kr (Y.-S. Lee).

https://doi.org/10.1016/j.jcis.2019.12.132
0021-9797/

1. Introduction

Energy storage sector improves the reliability and utilization of an electrical grid. Renewable and environmentally responsible energy storage solution requires high roundtrip efficiency, long cycle life, low maintenance, and flexible power energy characteristics are good for grid functions. Rechargeable batteries are considered for electrical grid applications. Such batteries find a wide spectrum of applications ranging from portable electronics to large scale energy storage applications [1,2]. Lithium-ion batteries (LIBs) are first commercialized by SONY in the 1990's by using the layered cathode, $LiCoO_2$ invented by Prof. J.B. Goodenough with graphitic anode [3,4]. Although, LIB is widely used for portable electronics, but extended as a potential power source towards the automotive industry in the recent past. Therefore, the estimated value of LIB usage is predicted as >95 billion USD in 2025, which leads to the larger consumption of lithium resources and subsequent rise in the price [5]. Utilizing sustainable energy resources is an economically affordable and environmentally safer option for future generations. Compared to lithium, sodium resources are abundant (e.g., the cost of Li_2CO_3 is 6600 USD/Mt, whereas Na_2CO_3 is 60 USD/Mt) and widely distributed on the earth surface. Sodium-ion based intercalation compounds are initially studied in the 1970's, but the interest gets subsided due to the rapid progress in the LIB development. Sodium-ion batteries (SIBs) share similar chemical properties with LIB system, and the distribution of sodium is 3–4 orders of magnitude higher than lithium [6-9]. The only bottleneck in the designing high power SIBs is the higher ionic radius of Na^+ (102 Å) compared to Li^+ (76 Å) leading to sluggish diffusion kinetics and higher volume change[10]. Graphite anode is the perfect example to understand the difference between the aforesaid two battery systems. The differences in atomic weight and ionic radius have a significant effect and influence on the cyclability and power capability of the battery system. The redox potential of Na^+ is slightly higher than Li^+. (−2.71 V *vs* −3.05 V *vs*. SHE) which reduces the overall cell voltage of SIBs [11,12]. Aluminium does not form an alloy with sodium; hence, it can be safely used as an anodic current collector compared to expensive Cu [13]. However, industrial production is still pushing to further improve the power capability and lifetime of the battery due to higher demand in various applications. Interfacial engineering is one of the best-pursued approaches in this direction since it influences both the power density and lifeline of the battery. Importantly, this modification certainly prevents inevitable side reactions at electrode and electrolyte at the positive side, which is the main cause for capacity fading. [14-17].

A wide range of cathode materials was studied as the promising host for SIBs like layered oxides, [14,18,18,19] polyanionic compound [20,20,20,20,20], organic compounds [21a,21b 22]. Among these, P2 type manganese-based layered oxides are more actively pursued due to its high theoretical capacity, more flexibility in design, and low-cost [23]. The P2 type layered oxides consist of two MO_2 layers build by edge-sharing MO_6 octahedral units. The Na^+ cation resides comfortably in the prismatic sites between these layers which come under one of the broad classifications of Delmas et al. [24,25]. However, the appearance of multiple voltage plateaus in the charge-discharge process, and Mn^{3+} dissolution resulting from Jahn-Teller distortion have been a serious concern over the years. Hence, the research activities are keen to replace the Mn^{3+} with several other metals with either iso or aliovalent substitutions to attain stable structures with better electrochemical properties [26].

Cation doping is a common and simple strategy to improve the rate capability of the LIB [27] and SIBs [28]. In our previous work, we have established that Al-doping can improve the structural stability of layered P2-$Na_{0.5}Mn_{0.5}Co_{0.5}O_2$ [29]. Also, the partial replacement of Mn with Co significantly improve the electrochemical properties of the cathode [30]. Even 10% of Co doping is reported to improve the structural stability of the layered oxides by Bucher et al. [31]. The extraction and re-insertion of Na^+ take place smoothly with the disappearance of step-like voltage profiles. The substitution of low valence Co^{2+} ions could increase the average oxidation state of Mn ions (e.g., Mn^{4+}), thereby enabling the structural stability of the phase by preventing Jahn-Teller dissolution of Mn^{3+} ions [32]. Secondly, the Ni and Co substitution for the Mn site is said to increase the diffusion coefficient of Na-ions and result in higher power capability [33]. Therefore, $Na_{2/3}Mn_{2/3}Co_{1/3}O_2$ is reported as a high capacity cathode and reversibly able to intercalate 0.5 mol of Na within 1.5 to 4.0 V window [34]. Wang et al. [34] performed a detailed study on the electrochemical performance of the $Na_{2/3}Mn_yCo_{1-y}O_2$ cathode at higher voltages and predicted that these layered oxides undergo severe structural transition at higher voltages. However, such high voltage (>4.2 V) P2-O2 phase transition induces the capacity fading and poor rate performance. Chen et al. designed an integrated P2/P3 $Na_{0.66}Mn_{0.5}Co_{0.5}O_2$ as a high rate cathode within the limited voltage of 1.5–4.3 V [35]. Wang et al. [36] utilized Co^{2+}/Co^{3+} redox couple for the first time in sodium layered oxides. Increasing the voltage window could increase the energy density of the layered oxides, but at the sacrifice of material stability subjecting to several factors. The electrode-electrolyte interface is a crucial factor in determining the safety and feasibility of the SIB at elevated temperatures. In common, electrolytes are made of Na^+ ion conducting salts dissolved in a mixture of carbonate-based organic solvents, which has low thermal stability with high volatility and flammability that limits the operating temperature and safety of SIBs [37,38]. Hence interfacial engineering is a must for better stability and safety at elevated temperatures.

Exploring new cathode materials with wide interlayers is one of the ways of designing high power cathode [18,39], whereas overcoming the setbacks of existing high capacity layered oxides in terms of structure or interfacial properties is another away of tackling the issue [19,40]. Herein, we adopt surface modification/interfacial engineering as the strategy to design high power layered oxides [41]. Initially, carbon coating is considered as one of the solutions to overcome the poor rate performance [42]. But, the carbon layer reduces the redox capacity of the cathode. In contrast, metal oxide coating certainly improves the rate performance along with yielding higher capacity [43]. Liu et al. [44] reported the Al_2O_3 coating over $Na_{0.67}Ni_{0.33}Mn_{0.67}O_2$ particulates *via* the sol-gel method. This solution coating method of Al_2O_3 encapsulates the surface of the individual particles, thereby increasing the electrical resistance and polarization of the cathode and the capacity is approaching zero at higher rates. Also, the solution coating process failed to provide a homogeneous coating.

Atomic layer deposition (ALD) is one of the successful and simple techniques employed uniform and conformal coating and convincingly validated for several li-ion battery electrodes [16]. It is well known that Al_2O_3-based coating is non-ideal due to the resistive nature of the oxide. However, for ultrathin layers of Al_2O_3, lithium can diffuse reasonably well through the layers [15,16,45]. The success of this method lies in the (i) very conformal coating on different active materials, (ii) able to control the thickness and (iii) versatility of coating, (iv) suppress CEI layer formation and acts an artificial CEI layer, (v) strengthen the electronic conductivity of the cathode by keeping it together, and (vi) act as a hydrofluoric acid (HF) scavenger [46]. Still, the potential application of this ALD process is at the initial stage of research. Recently, Karthikeyan et al. [43] conducted a conformal coating of Al_2O_3 by ALD as an artificial CEI layer and found that optimized surface

coating could improve the stability and rate capability of the cathode. On the other hand, more in-depth studies are needed to understand the effect of ALD coating on the electrochemical kinetics in SIBs. In this line, we studied the influence of Al_2O_3 coating thickness, (*i.e.,* the number of cycles) on the prefabricated electrodes of $Na_{0.5}Mn_{0.5}Co_{0.5}O_2$ using ALD. The necessary physical and chemical studies were performed and explained in detail.

2. Experimental section

2.1. Material synthesis

Modified Pechini method (MP) was used for the synthesis of micron-sized P2-type $Na_{0.5}Mn_{0.5}Co_{0.5}O_2$. In a typical process, a stoichiometric amount of sodium acetate (Sigma Aldrich, 99.5%), manganese acetate (Sigma Aldrich, 98%), cobalt acetate (Sigma Aldrich, 98%) were dissolved in distilled water. Then, the citric acid solution was added in a dropwise along with polyethylene glycol as a surfactant under vigorous stirring at 80 °C to encourage the esterification reaction. Ethylene glycol and conc. nitic acid was added to it, making the colour of the solution change to pink and subsequently dried. The dried precursor powder was subjected to pre-calcination at 500 °C in air. The intermediate product was again re-grinded well and fired at a high temperature of 900 °C in air. The final samples were named as MC900 and stored in the glovebox for further studies.

2.2. Atomic layer deposition (ALD) of Al_2O_3

A thin layer of Al_2O_3 film was deposited in a laminar-flow-type thermal ALD reactor (NCD, Lucida D100, Korea) on the prefabricated electrodes at the substrate temperature of 150 °C using trimethylaluminum (TMA) and de-ionized-H_2O as the Al and O sources, respectively. The TMA and H_2O sources were kept at 10 °C throughout the deposition process. A continuous flow of N_2 gas (50 sccm) was used as the carrier gas and for purging during the deposition process. The reaction scheme for one Al_2O_3 ALD cycle was set as follows: 0.5 s pulsing of TMA, 20 s purging of N_2, 0.5 s pulsing of H_2O, and 20 s purging of N_2. The repetition of the aforementioned sequence for two, five, and 10 cycles resulted in different thicknesses of the Al_2O_3 coating on the cathode materials. Hereinafter, the electrodes are denoted as MC900-0c, MC900-2c, MC900-5c, and MC900-10c, respectively.

2.3. Electrochemical characterization

Electrochemical studies were performed using standard CR2032 coin-type cells, adopting sodium metal as reference and counter electrode for half cells. The test cells were assembled in a glovebox in which the oxygen and hydrogen levels maintained at below 1 ppm. Whatman glass fiber paper was used as the separator, 1 M $NaClO_4$ in propylene carbonate with 2 vol% of fluoroethylene carbonate was used as the electrolyte. Each cathode consisted of 2.0 mg of accurately weighed active material, 0.5 mg of ketzen black, 0.5 mg of teflonized acetylene black (Table 1). The slurry of the above mixture was obtained with the assistance of ethanol and pressed over a stainless-steel mesh current collector and dried in a vacuum oven at 160 °C for 4 h. Charge-discharge studies were performed at different cut-off voltages (*vs.* Na) for various current rates using battery tester (WBS 3000, Won-A-Tech, Korea) at room temperature (25 °C) and high temperature (50 °C) conditions.

2.4. Material characterization

X-ray diffraction (XRD) pattern of the samples was obtained over the 2θ range of 5-90° at the scanning rate of 2° degree per min (Cu K_α radiation, Rint 1000, Rigaku, Japan). The elemental composition of the samples was obtained using inductively coupled plasma atomic energy spectroscopy (ICP-AES). X-ray photoelectron spectroscopy (XPS) was used to analyze the valance state of the elements (Multilab 2000, UK) on the surface. The morphology and microstructure of the samples were recorded using field emission scanning electron microscopy (FE-SEM, S-4700, Hitachi, Japan), energy dispersive spectroscopy and high-resolution transmission electron microscopy (HR-TEM; JEM-2000, EX-II, JEOL, Japan), respectively.

3. Result and discussion

The crystal structure of 50 cycles ALD Al_2O_3 coated MC900 is analyzed using XRD (Fig. 1a). Compared to other methods like the sol-gel method, the modified pechini (MP) synthesis process is highly facile resulting from the hydroxylation and condensation of the molecules that produce products of required structural and morphological features [47]. Here, the obtained peaks are very sharp which suggests the highly crystalline nature of the synthesized phase. There is no additional impurity peaks observed in the XRD pattern. The peak position well matches with P2 type crystal structure having hexagonal unit cell and P63/mm3 space group. Accordingly, the high intense reflections are labeled. Inset of Fig. 1a represents the crystal structure of P2-type sodium layered oxide which composed of MO_6 edge-sharing octahedral units together forming $(MO_2)_n$ sheets that can easily accommodate alkali ions in the prismatic position. This trigonal prismatic coordination of Na-ions is facing sharing each other and hence, facilitate direct Na-ion diffusion between sites resulting in the higher diffusion coefficient of these structures. The chemical composition of MC900 is confirmed as 0.49:0.511:0.489 using ICP-OES analysis and is matched with the calculated value. Fig. 1b is that of SEM analysis along with selected area electron diffraction (SAED) pattern provided as inset. Apparently, the synthesized particles are in few micrometers long with irregular shape as that of other reported P2-layered oxide cathodes. This kind of irregular morphology is quite common while employing the modified pechni process. The particles have very thin width resembling microplates. The SAED pattern exhibits a clear lattice spot with the hexagonal arrangement. All these confirm the phase purity and crystalline nature of the structure. Fig. 1c shows the HR-TEM image of the MC900 particle, which carefully separated from the prefabricated electrode showing a uniform surface layer after 50 cycles

Table 1
Values of resistance calculated from fitting the Impedance graphs.

Samples	Before Cycling			After Cycling		
	Rsol(Ω)	Rct(Ω)	Zw (Ω)	Rsol(Ω)	Rct(Ω)	Zw (Ω)
MC900-0c	20.53	2253.4	2368	13.66	293.43	252.2
MC900-2c	18.63	1729.94	455	17.833	267.59	184.7
MC900-5c	13.88	1416.79	297.5	10.215	257.02	138.9
MC900-10c	12.05	1783.8	439.8	11.016	224.92	156.3

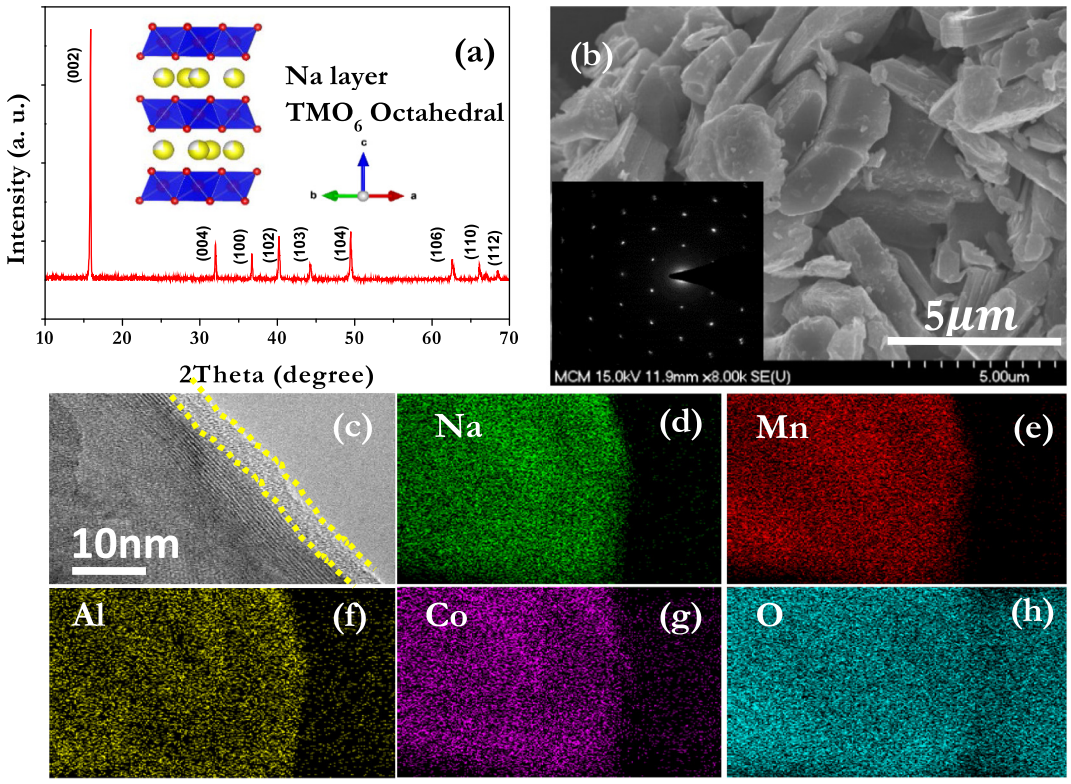

Fig. 1. (a) XRD peaks of 50 cycle ALD Al_2O_3 coated MC900 with its crystal structure (b) SEM image with SAED pattern (c–h) EDS elemental mapping of Al_2O_3 coated MC900.

of ALD Al_2O_3 coating. The conformal coating is very clear with amorphous nature and no influence on the structural aspects of the parent materials which is clearly seen from the absence of impure peaks in Fig. 1a. Fig. 1(d–h) shows the elemental mapping of Mn, Co, and Al recorded alongside TEM analysis. All the elements are uniformly distributed with a denser Al distribution at the surface of the particle. The HRTEM image of MC900 without ALD modification is provided in Fig.S1 for comparison and has no distinct surface coating seen.

XPS analysis (Fig. 2b) was carried out to elucidate the effect of ALD Al_2O_3 coating on the surface. To probe the effect of surface modification on the electrode surface, we performed *ex-situ* XPS analysis after varying the number of coating cycles. In the case of pristine electrode, a major peak of $Mn2p_{3/2}$ is convoluted into two minor bands located at 642.1 and 643.81 eV which belongs 3+ and 4+ valance state of Mn, respectively [41]. The peak positions are shifted towards lower binding energy with the increasing no of ALD cycles (2 and 5 cycles) due to the reduction in the average oxidation state. Similarly, the two main Co peaks of ALD Al_2O_3 coated electrodes can be disintegrated into four minor peaks located at 781.97, 797.96, 780.13 and 795.22 eV in which the former two representing Co^{2+} and the later that of Co^{3+} respectively [29]. Very interesting thing is that the electrode without ALD coating has only Co^{3+} peaks. Further, the average oxidation state of Co is also found to be reduced. This is because Mn^{4+} and Co^{3+} ions in the surface are being reduced by accepting electrons from the adsorbed Al ions forming a complex layer as reported for other works [15]. Al2p peak can be spotted at the binding energy of 75.23 eV for surface modified electrodes marking its presence on the electrode surface [29]. The effect of these changes on electrochemical performance is analyzed in the forthcoming sections.

The electrochemical performances of pristine and ALD coated electrodes were carried out using cyclic voltammetry (CV), galvanostatic charge-discharge (GCD) and electrochemical impedance spectroscopy (EIS). Fig. 3a shows the CV curves of pristine and

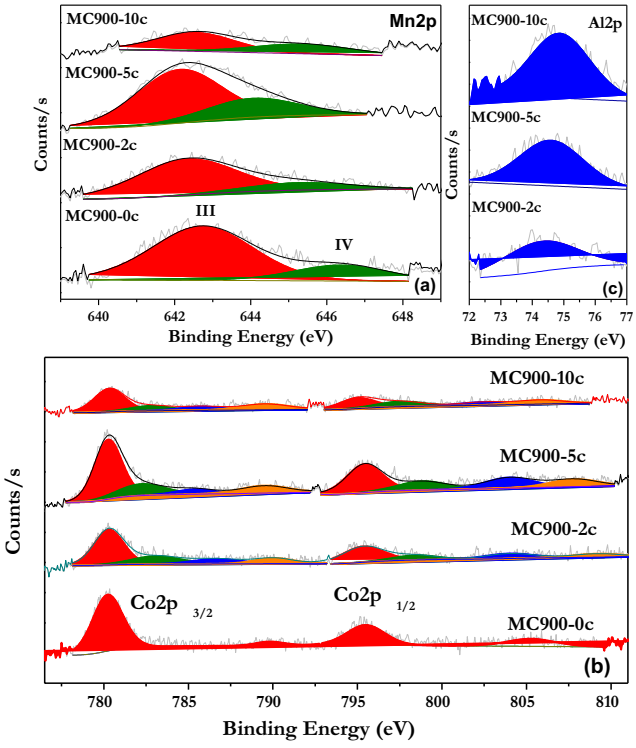

Fig. 2. De-convoluted XPS spectrum of pristine and different cycles of ALD coated MC900 (a) Mn, (b) Co, and (c) Al.

surface-modified electrodes for the first three cycles between 1.5 and 4.5 V *vs.* Na at 0.5 mV s^{-1}. Two pairs of redox peaks appear in all cycles due to the complex process involving the redox reaction of Mn and Co with varying valence states. During the

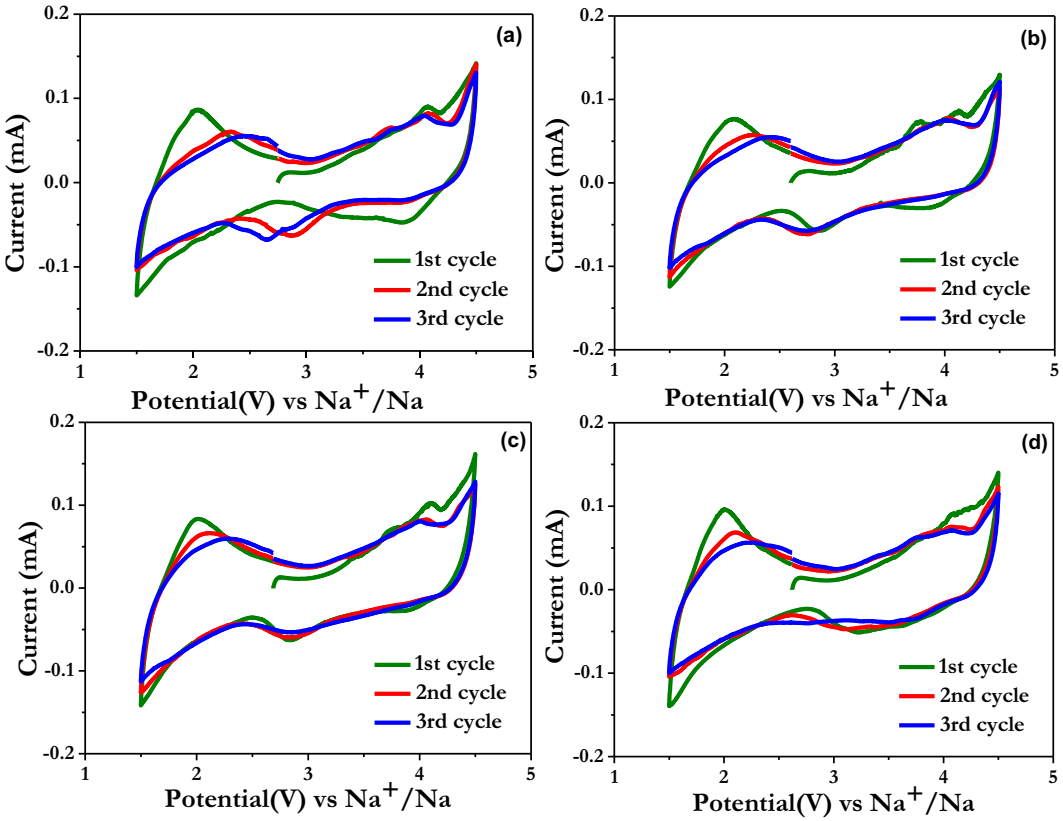

Fig. 3. CV curves of MC900 samples at 0.5 mV s^{-1} (a) Pristine, (b) 2 cycles of ALD Al_2O_3 coated, (c) 5 cycles of ALD Al_2O_3 coated, and (d) 10 cycles of ALD Al_2O_3 coated.

initial positive sweep, the redox peaks above 3.0 V *vs.* Na is due to the oxidation of Co^{3+} to Co^{4+} followed by two sets of reduction peaks around 4.0 and 2.0 V *vs.* Na due to the reduction of Co^{4+} and Mn^{4+} [35]. In the subsequent cycles, the redox peaks become unusual with the appearance of a new peak around 2.5 V *vs.* Na which is possibly originated from the $Co^{3+/2+}$ couples [35]. Obviously, the increase in voltage polarization with the gradual shift in reduction peaks are clearly seen as the cycling proceeds. The intensity of peak at 4.0 V *vs.* Na corresponding to $Co^{4+/3+}$ reduction is minimized with the simultaneous increase in the $Co^{3+/2+}$ couples around 2.5 V *vs.* Na. The CV traces of surface-modified electrodes using different thickness of ALD Al_2O_3 coating is compared with the above results to understand the changes taking place in the cell. All the electrodes show active participation of $Co^{3+/2+}$ redox during the discharge cycle. The electrode coated with 5 cycles of ALD Al_2O_3 is highly reversible in the consecutive cycles compared to the other three electrodes. Specifically, the pristine electrode shows a higher amount of deviation when compared to the surface-modified electrodes. In addition to the above peaks, when the electrodes are cycled to a higher voltage, especially to 4.5 V *vs.* Na, a sharp peak appears at ~4.4 V *vs.* Na representing slight electrolyte oxidation and formation of CEI layer on cathode interface [14]. Fig. 4 represents the galvanostatic charge-discharge curves of pristine and ALD coated cathode between 1.5 and 4.5 V *vs.* Na at varying current rates from 0.5 to 40 C rate (1 C = 136 mAh g^{-1}) for analyzing the stability and rate capability. Initial charge behavior is completely different from the subsequent cycles for all the electrodes. This is mainly because of sodium deficiency in the synthesized compounds as shown in ICP analysis [26]. The pristine electrode has an initial charge capacity of 111 mAh g^{-1} corresponding to 0.415 mol Na extraction from the cathode when charged to 4.5 V *vs.* Na due to $Co^{3+/4+}$ oxidation. During discharge, 0.58 mol Na inserted back to the cathode and delivering a high capacity of 156 mAh g^{-1} with the simultaneous reduction of $Mn^{4+/3+}$ and $Co^{4+/2+}$ as seen from the clear voltage plateau at around 2.5 V *vs.* Na. The second charge curve has a plateau below 2.5 V *vs.* Na possibly due to $Mn^{3+/4+}$ couple and simultaneous oxidation of $Co^{2+/3+}$ with plateau above 3.0 V *vs.* Na corresponds to the $Co^{3+/4+}$ process. However, the following cycles are showing slight capacity fading with the increasing separation between the charge and discharge voltage plateau's *i.e.*, an increase in polarization. Generally, the voltage fading may be due to the dissolution of Mn^{3+} ions during deeper discharge resulting in loss of active materials [44]. Further, it has been reported that, when the cells are discharged below 1.7 V *vs.* Na, the Mn^{3+} ions tend to distort the structure which regains the electronic stability and thereby initiating fading mechanism [36]. The 2, 5 and 10 cycles ALD Al_2O_3 coated cathode delivers a higher initial charge capacity of 122, 132 and 125 mAh g^{-1} which corresponds to the 0.45, 0.49 and 0.46 mol Na extraction. Similarly, a higher discharge capacity of 165 (0.61 mol Na), 175 (0.65 mol Na) and 168 mAh g^{-1} (0.62 mol Na) has resulted. Overall, 5 cycle ALD Al_2O_3 coated electrode exhibited better performance with very high capacity among the other Mn based layered oxides compared. Importantly, the voltage fade is significantly suppressed for surface modified samples in the consecutive cycles. The presence of low valance, high spin Co^{2+} at the end of discharge is said to maintain the average voltage of Mn slightly above 3+ which partially suppresses the Jahn-Teller distortion [36].Stability and rate capability are other important parameters for high power applications. Hence, all the electrodes were continually tested for varying currents from 0.5 C to 40 C between 1.5 and 4.5 V *vs.* Na, as shown in Fig. 5a. The capacity retained at high current rates is related to the charge transfer at the interface. Even though the performance of the pristine cathode is better than many reported cathodes due to its high crystallinity and uniform distribution of elements, the overall

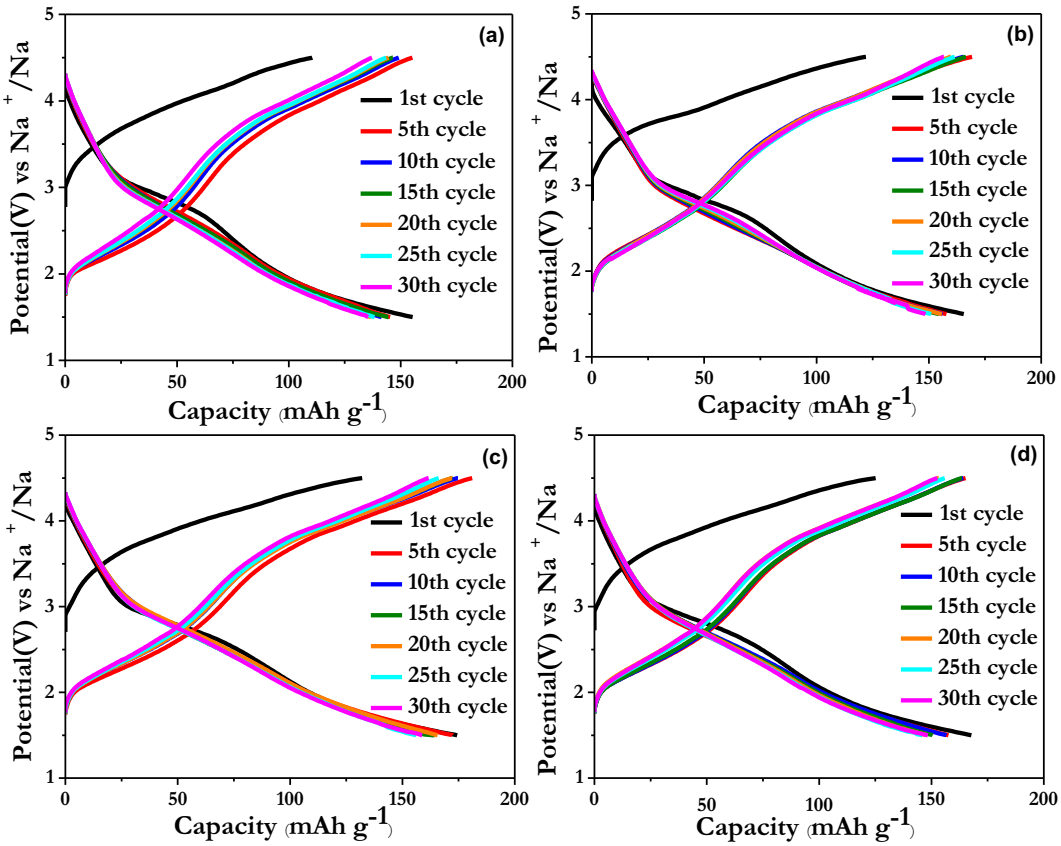

Fig. 4. Charge Discharge curves of MC900 (a) Pristine, (b) 2 cycles of ALD Al_2O_3 coated, (c) 5 cycles of ALD Al_2O_3 coated, and (d) 10 cycles of ALD Al_2O_3 coated.

performance can be further improved by modifying the interface with the ALD coating [35]. Also, charge-discharge curves resemble without distinct voltage plateau when the applied current is very higher due to insufficient time for bulk diffusion [48]. ALD modified electrodes show better performance than the pristine electrode at higher currents. Pristine electrode gives discharge capacity of 156, 118, 85, 67, 45 and 25 mAh g^{-1} at 0.5, 1, 5, 10, 20 and 40 C rates, respectively. Among varying cycles of ALD Al_2O_3 modification, the one with 5 cycle ALD coating has better performance with high discharge capacities at varying current rates. The discharge capacity of all the electrodes is found to be linearly decreasing with increasing current density due to polarization [30]. It is common that the electrode materials are subjected to high stress during the charge-discharge process, especially at high current rates. The improved performance of the optimized Al_2O_3 coated electrodes is due to the difference in bandgap energies between MC900 and the coating materials and high fracture toughness of 3.5 mPa m^{-2}. Al_2O_3 coating has a higher E_g value of 9.0 which prevents the electrons in the conduction band of the cathode to move into coating material and induce reactions [49]. Also, this layer acts as a flexible film that can accommodate stress and volume change. [50] The charge-discharge curves with varying current densities for pristine and surface modified cathodes are provided in Fig. S2. The above rate performance is higher than many reported P2-type cathode materials [58,58]. The stability of pristine and optimized 5 cycle coated electrodes are tested at 2 C rate between 1.5 and 4.5 V *vs.* Na and shown in Fig. 5e. The ALD Al_2O_3 coated electrode has a slightly higher capacity of 143 mAh g^{-1} with 79% capacity retention after 100 cycles, whereas the pristine can only retain 75% of its initial capacity.

The above results made it clear that only optimized coating is necessary for superior electrochemical performance. For increasing number of ALD Al_2O_3 cycles, the capacity tends to decrease as it is difficult for the ions to pass through the higher diffusion barrier of insulating Al_2O_3 [51]. All the electrodes could retain the capacity after cycling, making it highly reversible. The presence of Al_2O_3 coating is said to prevent the Mn^{3+} dissolution into electrolyte at deep discharge [44]. To our surprise, all the electrodes including pristine MC900 show a smooth curve above 4 V *vs.* Na without any predominant P2-O2 phase transition, which is a major problem in sodium deficient P2-layered oxides. To be clear, when more Na^+ ions are de-intercalated from the sodium layered oxides, the electrostatic repulsion between the adjacent oxygen layers causes phase transition from P2-O2 through slab gliding, causing partial irreversibility and capacity fading over cycles [48]. As mentioned, the phase transition at higher voltages is a serious problem for layered oxides, as it collapses the structure at the interface, thereby blocking the Na^+ diffusion pathways. The P2-O2 phase transition accounts for about 15% volume shrinkage compared to 2% volume change of pure P2-phase [50]. This high stress resulting from volume change impose kinetic limitations. Within the voltage window of 1.5–4.5 V *vs.* Na, many factors tend to affect the performance of layered oxides. (i) Electrolyte oxidation above 4.3 V *vs.* Na could be triggered due to the presence of highly acidic HF species in the electrolyte and increased interfacial reactions at elevated temperature created by highly oxidizing environments which result in the thick insulating CEI layer. This eventually consumes more Na^+ ions in an irreversible manner, which causes a reduction in the initial coulombic efficiency and higher interfacial impedance [14,52]. (ii) irreversible loss of oxygen ions from surface lattice is a concern [53]. (iii) disproportionate reaction of Mn^{3+} into Mn^{2+} and Mn^{4+} below 1.7 V *vs.* Na causes active metal dissolution and the resulting Jahn-Teller distortion to achieve electrochemical stability [19]. Hence, the bare electrode has serious capacity fading

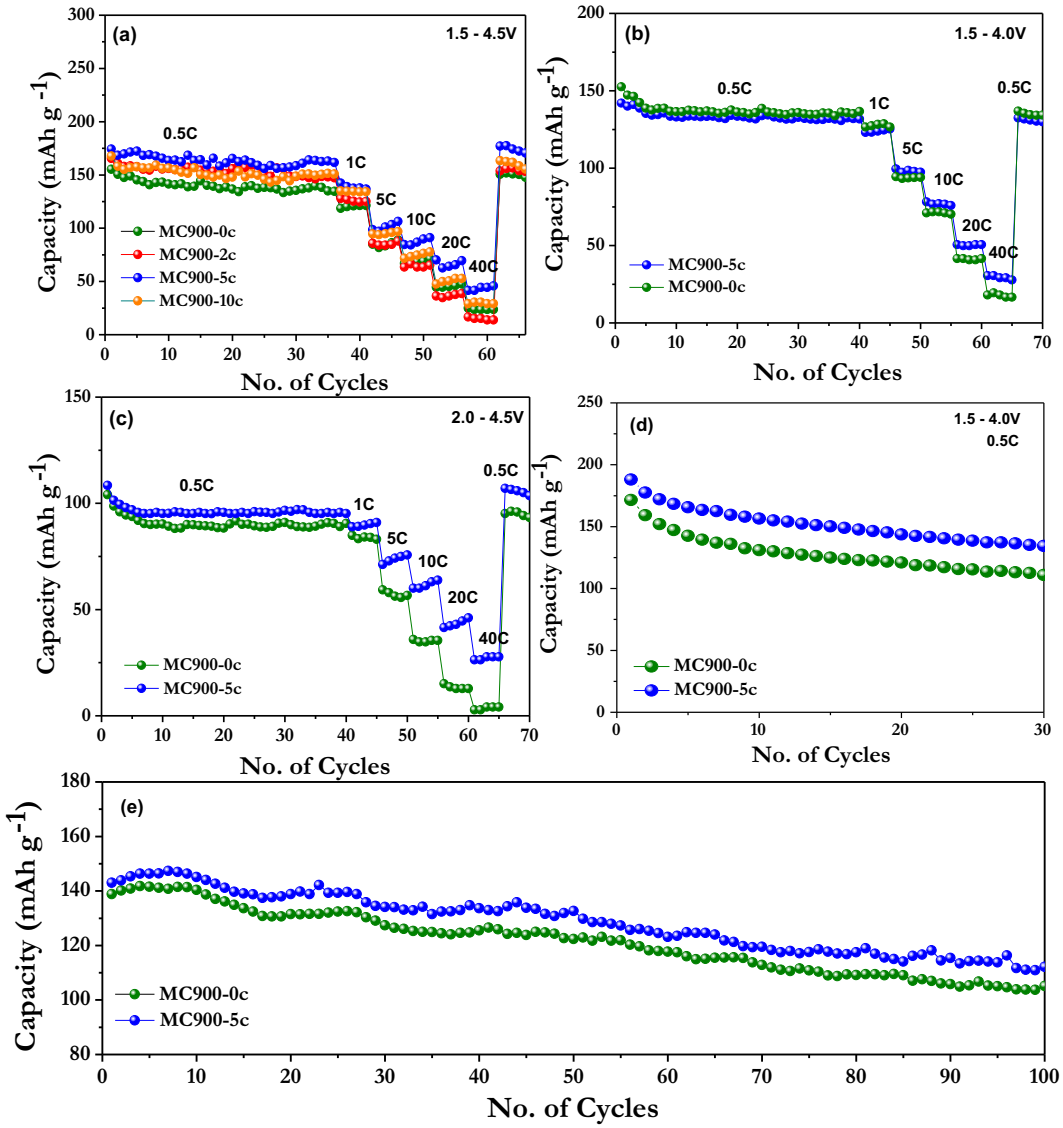

Fig. 5. Cyclability and Rate performance of Pristine and ALD Al_2O_3 coated MC900 within different cutoff voltages (a) 1.5–4.5 V *vs.* Na (b) 1.5–4.0 V *vs.* Na (c) 2.0–4.5 V *vs.* Na, (d) Cyclability of MC900 between 1.5 and 4.0 V at high temperature (50 °C), and (e) Cyclability of pristine and MC900 between 1.5 and 4.5 V *vs.* Na at room temperature.

at higher currents resulting in poor capacity retention characteristics. Modifying the interface using an optimum number of ALD cycles certainly avoids the direct contact of electrode active materials with electrolyte, and thereby stabilizing the electrolyte decomposition above 4.3 V *vs.* Na [52]. The loss of active materials by dissolution is suppressed over prolonged cycling. All these together contribute to a higher capacity as well as improved rate capability of surface-modified electrodes. Moreover, the cells could recover its almost complete capacity when cycled back to 0.5 C rate after 40 C.

Hence, it is better to understand the contribution of these drawbacks individually. Initially, we fixed the lower cutoff voltage at 2.0 V *vs.* Na and higher at 4.5 V *vs.* Na (Fig. 5c). Here, we intentionally overcharge MC900 up to 4.5 V *vs.* Na to examine the solvent oxidation and its influence on cathode kinetics. This excludes the structural disturbance caused by Mn at deep discharge while specifically focusing on high voltage electrolyte decomposition and structural transformation. The initial capacity in this voltage range is 108 mAh g^{-1} and 104 mAh g^{-1} for MC900-5c and MC900-0c at a current rate of 0.5 C. In this voltage range, only single plateau is observed during charging and discharging involving $Co^{2+}/Co^{3+}/Co^{4+}$ redox pair with higher average voltage plateau of 2.9 V *vs.* Na [36] (Fig. S3c,d). Irrespective of ALD Al_2O_3 surface modification, both the electrodes show better stability with >99% capacity retention after 70 cycles. In terms of rate performance, as the applied current rate increases from 1 to 40 C, the pristine material gives a capacity of 85, 59, 36, 15 and almost reached 2.7 mAh g^{-1}. On the other hand, under similar circumstances, the 5 cycle ALD Al_2O_3 modified cathode gives higher rate performance with 89, 71, 60, 42 and 26 mAh g^{-1}, respectively. Oxidation of electrolytes takes place when the cathode voltage raises above its LUMO until a uniform and stable layer of CEI is formed. Stable CEI layer with high ionic conductivity, better chemical, mechanical and electrochemical stability along with lower electronic conductivity is favorable for better performance [52]. The effect of CEI layer can be understood from the initial coulombic efficiency values of pristine and coated electrodes. Creating an artificial CEI layer is more protective for high voltage cathodes of future SIBs. Here, ALD Al_2O_3 coating with 5 cycles acts as an artificial CEI layer towards translating superior power capability. Thus, the improved performance in this voltage range is attributed to the stable CEI layer formation after ALD modification, allowing better Na^+ ion

kinetics at the higher current rate. Foremost, Al_2O_3 coating is an insulator for electrons across the interface, but prevent direct contact of the electrolyte with the electrode active material over prolonged cycles. All these have a cumulative effect on the high voltage operation of the cathode. Thus, interfacial modification using conformal Al_2O_3 coating is an efficient way of developing high voltage cathode for SIB.

It is well known that Jahn-Teller distortion and the Mn-based structural distortion is predominant during the deep discharge process. This leads to the dissolution of Mn^{2+} ions into electrolyte after consecutive cycles [54]. Therefore, by restricting the upper cut-off voltage to 4.0 V *vs.* Na, we can exclude the capacity fading contribution from electrolyte decomposition and structural transition at higher voltages (Fig. 5b). Limiting the cut-off voltage improves cyclability and initial coulombic efficiency due to single-phase reaction at the expense of capacity. In this case, the pristine material has a high initial capacity of 152 mAh g^{-1} compared to ALD modified cathode with 142 mAh g^{-1}. The stability is very excellent irrespective of ALD coating with 92% and 88% capacity retention for MC900-5c and MC900-0c after 70 cycles. Again, the significance of ALD coating comes into play at the higher current rate with MC900-5c retaining 51 and 31 mAh g^{-1} at 20 and 30C rates, respectively. Two sloping voltage profiles centered on 2 V *vs.* Na and 3.5 V *vs.* Na are clearly seen in the charge-discharge curves (Fig. S3a-b). These are the contribution from the $Mn^{3+/4+}$ and $Co^{3+/4+}$ couple for a very high capacity [35]. When the upper cut-off voltage is restricted to 4.0 V *vs.* Na, $Co^{3+/4+}$ redox is highly reversible both at room temperature and high temperature as seen below. More detailed studies are needed to understand these intrinsic effects of redox couples. The coulombic efficiency of pristine and ALD modified electrodes within different cut-off voltage are provided in Fig. S4(a–c).

Fig. 5d and S5 show the electrochemical studies of MC900-0c and MC900-5c at an elevated temperature of 50 °C between 1.5 and 4.0 V *vs.* Na. The charge–discharge curves represent the contribution of Co and Mn redox couples. MC900-0c and MC900-5c deliver a high capacity of 172 and 188 mAh g^{-1} at 0.5C rate. Despite its high capacity, it can be clearly seen that the degradation is very high at elevated temperature compared to room temperature performance. This is due to accelerated electrolyte decomposition and the high reducing ability of Mn^{4+} resulting in capacity fade [55]. This, in turn, causes further Mn dissolution in the consecutive cycles. The 5 cycles ALD Al_2O_3 coated electrode could retain 68% of initial capacity (128 mAh g^{-1}) after 30 cycles. This is due to the multiple roles of interfacial engineering by using amphoteric Al_2O_3 coating as the best scavengers of electrolyte byproducts [43]. ALD Al_2O_3 coating on powders or electrodes has effectively improved the cycle life and stability of several lithium-based electrodes at higher operating potentials. In all these cases, Al_2O_3 is perceived to be a discrete layer on the surface of the powder. Takashi et al. [43] clearly demonstrated that Al_2O_3 coating on the prefabricated electrode of $LiCoO_2$ could dope the Al without the necessity of post-deposition annealing. This improves the electrochemical performance of the cathode even at higher charge discharge rates. This is because a thin uniform monolayer of Al_2O_3 coating is said to form after approximately 10 ALD cycles. During the initial few cycles of ALD coating, Al from TMA bonds to the surface oxygen by consuming Mn-O and Co-O bonds [15]. At this stage, Al is almost like surface dopant than coating. This can be confirmed by the XPS studies in Fig. 2, where the average oxidation state of Mn and Co are reduced. This accounts for the superior rate performance of the 5 cycle ALD coating. In general, an annealing process is necessary to overcome the activation barrier for Al diffusion into the structure. However, in this case, the surface reactive sites created when the electrodes are exposed to the surface are few nanometers in thickness. These sites are highly reactive and undergo a self-limiting chemical reaction with TMA during coating, thus accounting for the graded incorporation of Al on the surface [43]. It's been said that diffusion of Na^+ ion is faster in the $Na_xAl_2O_3$ than that of Li^+ in $Li_xAl_2O_3$ as Na ion transport happens by hopping between O rich trapping sites *via* a Na-O bond-breaking making [56]. Weaker Na-Al-O boding can accommodate higher volume change during repeated charge-discharge cycles. Also, Na^+ diffusion through Al_2O_3 is said to induce low stress because of both vibrational and translational motion [56]. All these accounts for improved electrical conductivity together with the structural stability of active materials. Sol-gel coating of Al_2O_3 on the P2-$Na_{2/3}Ni_{1/3}Mn_{2/3}O_2$ will exhibit better stability, but the poor rate capability remains an issue which is mainly because of the coating thickness is uncontrolled and non-uniform. This often leads to the formation of the very thick protective layer (>12 nm) [44]. Similarly, 1 nm thick ALD Al_2O_3 coating on P2-$N_{2/3}Ni_{1/3}M_{2/3}O_2$ has experienced similar features with better stability with poor rate capability. However, the authors didn't clear about the coating cycles and other parameters which makes it difficult to consider for comparison [45]. Karthikeyan et al. [51] studied different cycles of ALD Al_2O_3 coating on P2-$Na_{0.67}Mn_{0.54}N_{i0.13}Co_{0.13}O_2$, where less than 1 nm coating is having superior stability and rate performance justifying our results. The fundamental understanding of the ALD Al_2O_3 coating of Na-based layered oxides is proposed based on our results. It shows that ALD Al_2O_3 can significantly improve the power capability of the cathode irrespective of its insulating nature. Hence, ALD Al_2O_3 coating on sodium layered oxides can be considered for significant development of cathode materials for advanced sodium-Ion Batteries with high power capability. Fig. 6 shows the schematic of half cell with ALD Al_2O_3 modified MC900 and Na-metal anode during discharge along with the scheme of the surface coating layer.

Impedance is a powerful tool to understand the interfacial properties of the cathode with and without ALD Al_2O_3 modification. Hence, we have performed the electrochemical impedance spectroscopic (EIS) studies before cycling for electrodes coated with different cycles of ALD Al_2O_3 coating and provided in Fig. 7 (a). The graphs are fitted using the equivalent circuit provided in Fig. 7a and the corresponding resistance values are provided in Table.S1. Initially, the cells are fabricated and kept at aging for a few hours to stabilize the interface. The EIS spectra have two parts, one semicircle from high-frequency region to medium frequency region and a sloping line at the low-frequency region. The semicircle is because of the combined phenomenon of two reactions with similar time constants (*i.e.,* the surface film resistance and the charge-transfer resistance). The sloping line is the diffusion resistance in the bulk of the cathode [57]. The decreased charge transfer resistance of the ALD Al_2O_3 modified electrodes compared to the bare electrode is due to the improved interfacial properties after surface treatment. This observation could not be seen if a significant thickness of a highly resistive coating like Al_2O_3 was present. This is clearly justified by the charge-discharge studies conducted above. After subjecting to cycling studies at different current rates, the EIS is again recorded and displayed in the Fig. 7(b). The Nyquist plot after cycling shows a clear difference between the ALD Al_2O_3 modified and pristine cathode. This is due to the unstable CEI layer and the resulting structural damage at the interface after reaction with the electrolyte. The formation of the CEI layer induced by electrolyte oxidation is the only major bottleneck for the pristine electrode inducing larger charge transfer resistance before and after cycling [52]. The 2 and 5 cycles ALD Al_2O_3 coated electrodes have partially covered Al precursors on the surface like surface doping of Al rather than coating and help to stabilize the CEI layer formed on the interface, resulting in very low charge transfer resistance before and after cycling. The maximum thickness of the coat-

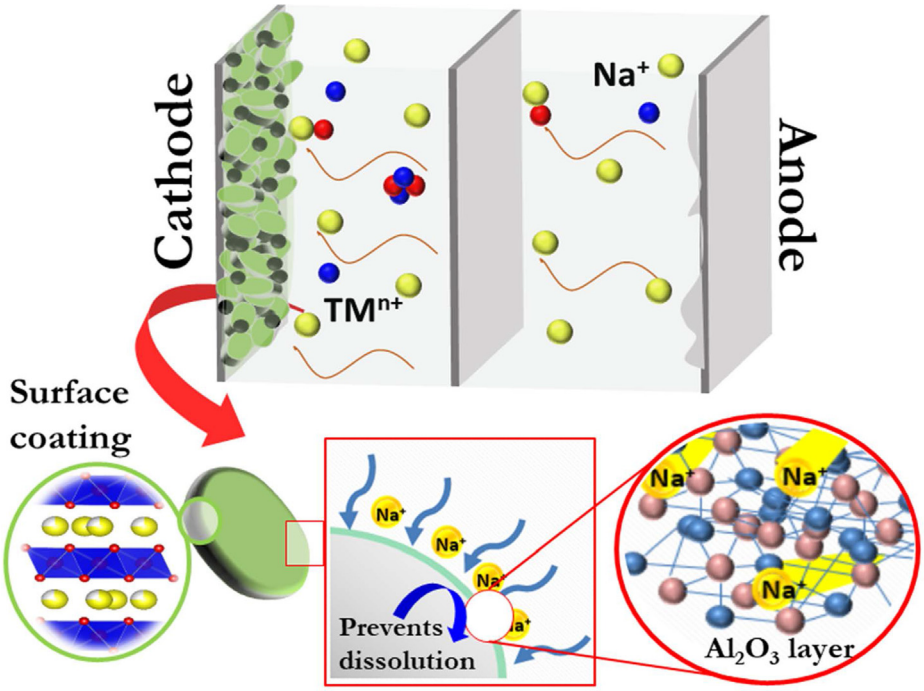

Fig. 6. Schematic of the half cell with ALD Al_2O_3 modified MC900 and Na-metal anode during discharge along with the scheme of the surface coating layer.

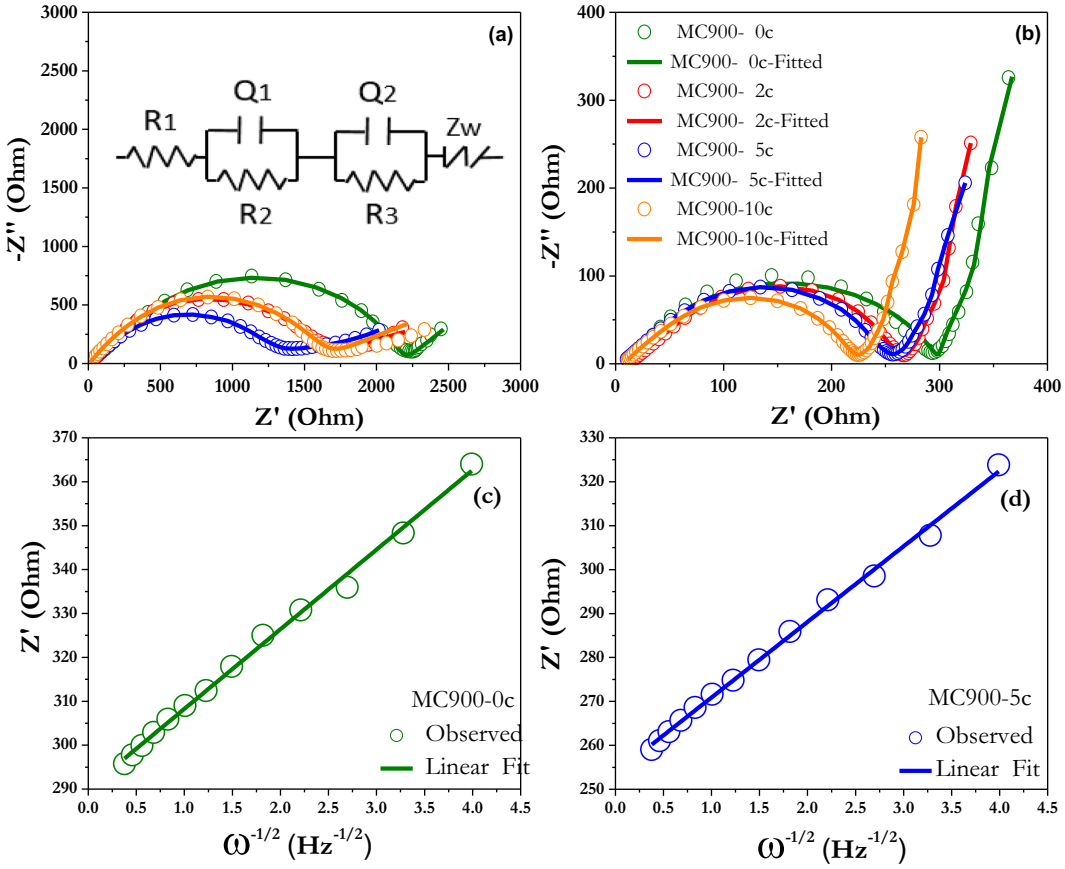

Fig. 7. Nyquist plot of Pristine and ALD Al_2O_3 coated MC900 (a) Before (inset shows the equivalent circuit used for fitting) and (b) after cycling (c,d) Randles plot between the real plot of impedance *vs* the inverse square root of frequency measured after cycling for both MC900-0c and MC900-5c respectively.

ing layer in this work does not exceed 1 nm (10 cycles of ALD Al_2O_3 corresponding to one single layer of conformal coating). This creates an additional bottleneck for ion diffusion resulting in slightly higher interfacial resistance for a 10 cycle coated electrode before cycling. In contrast, the impedance measured after cycling has its interfacial resistance inversely proportional to no of cycles of ALD Al_2O_3 coating. This is because all kinds of degradation mechanisms come into play during cycling which severely affects the less coated. The diffusion coefficient of the Na-ions was calculated from Impedance spectra after cycling using the following equation [59],

$$D_{Li} = \frac{R^2T^2}{2A^2n^4F^4C^2\sigma^2} \quad (1)$$

where, σ is the Warburg factor, R is the gas constant, A is the area of the electrode, F is the Faraday constant, C is the concentration of sodium ions in the electrode material and *n* is the number of electrons involved in the reaction. The Warburg factor is obtained from the slope of the linear plot between the real part of the impedance and the inverse square root of the frequency at low-frequency regions [Fig. 7(c, d)] using the following relation,

$$Z' = R_s + R_{ct} + \sigma_w\omega^{-1/2} \quad (2)$$

The diffusion coefficient values of MC900-0c and MC900-5c are 47.4×10^{-12} and 63.2×10^{-12} cm^2 s^{-1}. This shows that 5 cycles of ALD coated MC900 has a higher diffusion coefficient than the pristine electrode without coating. Therefore, conformal surface modification can play a major role in the electrochemical process by protecting the dissolution of active particles and the improved interface. This helps in designing high power SIBs with higher upper cut-off voltages.

4. Conclusion

P2-$Na_{0.5}Mn_{0.5}Co_{0.5}O_2$ utilizing $Co^{3+/2+}$ redox couples were synthesized using polyol synthesis and studied as a high-power cathode for SIBs. We performed interfacial engineering using different cycles of ALD Al_2O_3 coating and studied its effects on electrochemical kinetics. Surface coating with ALD Al_2O_3 reduced the average oxidation state of Mn and Co ions. The 5 cycles of ALD modified electrode delivers a high capacity of 174 mAh g^{-1} and have superior rate capability irrespective of the applied voltage window. Even at 40C, the cathode delivers a high capacity of 45 mAh g^{-1}. Surface modification suppresses the electrolyte oxidation at higher voltages and stabilizes the CEI layer formed on the surface thereby reduced the charge-transfer resistance. The surface film, CEI acts as a buffer layer to volume expansion at higher current density leading to better stability even at high temperatures.

CRediT authorship contribution statement

Hari Vignesh Ramasamy: Conceptualization, Methodology, Writing - original draft. **Pravin N. Didwal:** Visualization, Investigation. **Soumyadeep Sinha:** Formal analysis, Resources. **Vanchiappan Aravindan:** Formal analysis. **Jaeyeong Heo:** Formal analysis. **Chan-Jin Park:** Formal analysis. **Yun-Sung Lee:** Supervision, Writing - review & editing, Project administration, Funding acquisition.

Declaration of Competing Interest

The authors declare that they have no known competing financial interests or personal relationships that could have appeared to influence the work reported in this paper.

Acknowledgement

The authors gratefully acknowledge the financial support from the National Research Foundation of Korea (NRF) grant funded by the Korean government (Ministry of Science, ICT & Future Planning) (No. 2019R1A2C1007620).

Appendix A. Supplementary material

Supplementary data to this article can be found online at https://doi.org/10.1016/j.jcis.2019.12.132.

References

[1] B. Dunn, H. Kamath, J. Tarascon, For the grid : a battery of choices, Science 334 (2011) 928–935, https://doi.org/10.1126/science.1212741.
[2] M. Armand, J.M. Tarascon, Building better batteries, Nature 451 (2008) 652–657, https://doi.org/10.1038/451652a.
[3] K. Mizushima, P.C. Jones, P.J. Wiseman, J.B. Goodenough, LixCoO2 (0<x<1): A new cathd e material for batteries of high energy density, Solid State Ionics. 3/4 (1981) 171–174.
[4] M.G.S.R. Thomas, P.G. Bruce, J.B. Goodenough, AC impedance analysis of polycrystalline insertion electrodes: application to $Li_{1-x}CoO_2$, J. Electrochem. Soc. 132 (2006) 1521–1528, https://doi.org/10.1149/1.2114158.
[5] Avicenne. Lithium ion battery raw material supply and demand 2016–2025. AABC Europe Jan 2017. Available from.Accessed April 23, 2018. http://cii-resource.com/cet/AABE-03-17/Presentations/BRMT/Pillot_Christophe.pdf.
[6] T.R. Jow, L.W. Shacklette, M. Maxfield, D. Vernick, The role of conductive polymers in alkali-metal secondary electrodes, J. Electrochem. Soc. 134 (2006) 1730–1733, https://doi.org/10.1149/1.2100746.
[7] M.S. Whittingham, Chemistry of intercalation compounds: Metal guests in chalcogenide hosts, Prog. Solid St. Chem. 12 (1978) 41–99, https://doi.org/10.1016/0079-6786(78)90003-1.
[8] C. Delmas, J.J. Braconnier, C. Fouassier, P. Hagenmuller, Electrochemical intercalation of sodium in Na_xCoO_2 bronzes, Solid State Ionics. 3 (4) (1981) 165–169.
[9] K.M. Abraham, Intercalation electrodes for rechargeable sodium cells, Solid State Lonics. 7 (1982) 199–212.
[10] A.S. Nagelberg, W.L. Worrell, A thermodynamic study of sodium-intercalated TaS_2 and TiS_2, J. Solid State Chem. 29 (1979) 345–354, https://doi.org/10.1016/0022-4596(79)90191-9.
[11] S.Y. Hong, Y. Kim, Y. Park, A. Choi, N.S. Choi, K.T. Lee, Charge carriers in rechargeable batteries: Na ions vs. Li ions, Energy Environ. Sci. 6 (2013) 2067–2081, https://doi.org/10.1039/c3ee40811f.
[12] C. Fang, Y. Huang, W. Zhang, J. Han, Z. Deng, Y. Cao, H. Yang, Routes to high energy cathodes of sodium-ion batteries, Adv. Energy Mater. 6 (2016) 1501727, https://doi.org/10.1002/aenm.201501727.
[13] Barker J, Wright CJ, inventors; Faradion Ltd., assignee. Storage and/or transport of sodium ion cells. WO/2016/027082. Filing Date 08/18/2015; 2016
[14] L. Mu, X. Feng, R. Kou, Y. Zhang, H. Guo, C. Tian, C.J. Sun, X.W. Du, D. Nordlund, H.L. Xin, F. Lin, Deciphering the cathode-electrolyte interfacial chemistry in sodium layered cathode materials, Adv. Energy Mater. 8 (2018) 1801975, https://doi.org/10.1002/aenm.201801975.
[15] L. Chen, R.E. Warburton, K.S. Chen, J.A. Libera, C. Johnson, Z. Yang, M.C. Hersam, J.P. Greeley, J.W. Elam, Mechanism for Al_2O_3 atomic layer deposition on $LiMn_2O_4$ from in-situ measurements and ab-initio calculations, Chem. 4 (2018) 2418–2435, https://doi.org/10.1016/j.chempr.2018.08.006.
[16] M.R. Laskar, D.H.K. Jackson, S. Xu, R.J. Hamers, D. Morgan, T.F. Kuech, Atomic layer deposited MgO: a lower overpotential coating for $Li[Ni_{0.5}Mn_{0.3}Co_{0.2}]O_2$ Cathode, ACS Appl. Mater. Interf. 9 (2017) 11231–11239, https://doi.org/10.1021/acsami.6b16562.
[17] T. Teranishi, Y. Yoshikawa, M. Yoneda, A. Kishimoto, J. Halpin, S. O'Brien, M. Modreanu, I.M. Povey, Aluminum interdiffusion into $LiCoO_2$ using atomic layer deposition for high rate lithium ion batteries, ACS Appl. Energy Mater. 1 (2018) 3277–3282, https://doi.org/10.1021/acsaem.8b00496.
[18] (a) D. Tie, G. Gao, F. Xia, R. Yue, Q. Wang, R. Qi, B. Wang, Y. Zhao, Modulating the interlayer spacing and Na+/vacancy disordering of P2-Na0.67MnO2 for fast diffusion and high-rate sodium storage, ACS Appl. Mater. Interfaces. 11 (2019) 6978–6985, https://doi.org/10.1021/acsami.8b19134;
(b) S. Bao, S. Luo, Z. Wang, S. Yan, Q. Wang, Improving the electrochemical performance of layered cathode oxide for sodium-ion batteries by optimizing the titanium content, J. Coll. Interf. Sci. 544 (2019) 164–171, https://doi.org/10.1016/j.jcis.2019.02.094.
[19] Y. You, S. Xin, H.Y. Asl, W. Li, P.F. Wang, Y.G. Guo, A. Manthiram, Insights into the improved high-voltage performance of Li-incorporated layered oxide cathodes for sodium-ion batteries, Chem. 4 (2018) 2124–2139, https://doi.org/10.1016/j.chempr.2018.05.018.
[20] (a) T. Broux, F. Fauth, N. Hall, Y. Chatillon, M. Bianchini, T. Bamine, J. Leriche, E. Suard, D. Carlier, Y. Reynier, L. Simonin, C. Masquelier, L. Croguennec, High rate performance for carbon-coated Na3V2 (PO4) 2F3 in na-ion batteries, Small Meth. 3 (2019) 1800215, https://doi.org/10.1002/smtd.201800215;

(b) Y. Zhao, X. Cao, G. Fang, Y. Wang, H. Yang, S. Liang, A. Pan, G. Cao, Hierarchically carbon-coated Na 3V2 (PO4)3 nanoflakes for high-rate capability and ultralong cycle-life sodium ion batteries, Chem. Eng. J. 2 (2018) 162–169, https://doi.org/10.1016/j.cej.2018.01.088;
(c) P. Feng, W. Wang, J. Hou, K. Wang, S. Cheng, K. Jiang, A 3D coral-like structured NaVPO 4 F/C constructed by a novel synthesis route as high-performance cathode material for sodium-ion battery, Chem. Eng. J. 353 (2018) 25–33, https://doi.org/10.1016/j.cej.2018.07.114;
(d) X. Li, S. Wang, X. Tang, R. Zang, P. Li, P. Li, Z. Man, C. Li, S. Liu, Y. Wu, G. Wang, Porous Na 3 V 2 (PO4)3/C nanoplates for high-performance sodium storage, J. Coll. Interf. Sci. 539 (2019) 168–174, https://doi.org/10.1016/j.jcis.2018.12.071;
(e) K. Liu, P. Lei, X. Wan, W. Zheng, X. Xiang, Cost-effective synthesis and superior electrochemical performance of sodium vanadium fluorophosphate nanoparticles encapsulated in conductive graphene network as high-voltage cathode for sodium-ion batteries, J. Coll. Interf. Sci. (2018), https://doi.org/10.1016/j.jcis.2018.07.114.

[21] (a) Y. Xu, M. Zhou, Y. Lei, Organic materials for rechargeable sodium-ion batteries, Mater. Today. 21 (2018) 60–78, https://doi.org/10.1016/j.mattod.2017.07.005;
(b) D. Wu, F. Jing, X. Xi, L. Ma, D. Lu, P. Yang, R. Liu, An Acid-Pasting Approach Towards Perylenetetracarboxylic Diimide Based Lithium/Sodium Ion Battery Cathodes with High Rate Performances, J. Coll. Interf. Sci. (2018), https://doi.org/10.1016/j.jcis.2018.11.085.

[22] W.J. Li, S.L. Chou, J.Z. Wang, Y.M. Kang, J.L. Wang, Y. Liu, Q.F. Gu, H.K. Liu, S.X. Dou, Facile method to synthesize na-enriched $Na_{1+x}FeFe(CN)_6$ frameworks as cathode with superior electrochemical performance for sodium-ion batteries, Chem. Mater. 27 (2015) 1997–2003, https://doi.org/10.1021/cm504091z.

[23] M.H. Han, E. Gonzalo, G. Singh, T. Rojo, A comprehensive review of sodium layered oxides: Powerful cathodes for Na-ion batteries, Energy Environ. Sci. 8 (2015) 81–102, https://doi.org/10.1039/c4ee03192j.

[24] C. Delmas, C. Fouassier, P. Hagenmuller, Structural classification and properties of the layered oxides, Phys. B+C. 99 (1980) 81–85, https://doi.org/10.1016/0378-4363(80)90214-4.

[25] X. Ma, H. Chen, G. Ceder, Electrochemical properties of monoclinic $NaMnO_2$, J. Electrochem. Soc. 158 (2011) A1307, https://doi.org/10.1149/2.035112jes.

[26] J.Y. Hwang, J. Kim, T.Y. Yu, Y.K. Sun, A New P2-type layered oxide cathode with extremely high energy density for sodium-ion batteries, Adv. Energy Mater. 9 (2019) 1803346, https://doi.org/10.1002/aenm.201803346. 1-10.

[27] P. Suresh, A.K. Shukla, N. Munichandraiah, Electrochemical properties of $LiMn_{1-x}M_xO_2$ (M=Ni, Al, Mg) as cathode materials in lithium-ion cells, J. Electrochem. Soc. 152 (2005) A2273–A2280, https://doi.org/10.1149/1.2073067.

[28] J. Billaud, G. Singh, A.R. Armstrong, E. Gonzalo, V. Roddatis, M. Armand, T. Rojo, P.G. Bruce, $Na_{0.67}Mn_{1-x}Mg_xO_2$ ($0 \leq x \leq 0.2$): a high capacity cathode for sodium-ion batteries, Energy Environ. Sci. 7 1387–1391 (2014), https://doi.org/10.1039/c4ee00465e.

[29] H.V. Ramasamy, K. Kaliyappan, R. Thangavel, W.M. Seong, K. Kang, Z. Chen, Y.S. Lee, Efficient method of designing stable layered cathode material for sodium ion batteries using aluminum doping, J. Phys. Chem. Lett. 8 (2017) 5021–5030, https://doi.org/10.1021/acs.jpclett.7b02012.

[30] C. Zhou, L. Yang, C. Zhou, B. Lu, J. Liu, L. Ouyang, R. Hu, J. Liu, M. Zhu, Co-Substitution enhances the rate capability and stabilizes the cyclic performance of O3-type cathode NaNi $_{0.45-x}$ Mn $_{0.25}$ Ti $_{0.3}$ Co $_x$ O $_2$ for sodium-ion storage at high voltage, ACS Appl. Mater. Interf. 11 (2019) 7906–7913.

[31] N. Bucher, S. Hartung, J.B. Franklin, A.M. Wise, L.Y. Lim, H.Y. Chen, J.N. Weker, M.F. Toney, M. Srinivasan, P2-$Na_xCo_yMn_{1-y}O_2$ (y = 0, 0.1) as cathode materials in sodium-ion batteries - effects of doping and morphology to enhance cycling stability, Chem. Mater. 28 (2016) 2041–2051, https://doi.org/10.1021/acs.chemmater.5b04557.

[32] J.H. Cheng, C.J. Pan, J.F. Lee, J.M. Chen, M. Guignard, C. Delmas, D. Carlier, B.J. Hwang, Simultaneous reduction of Co^{3+} and Mn^{4+} in P2 $Na_{2/3}Co_{2/3}Mn_{1/3}O_2$ As evidenced by X-ray absorpsion spectroscopy during electrochemical sodium intercalation, Chem. Mater. 26 (2014) 1219–1225, https://doi.org/10.1021/cm403597h.

[33] D. Yuan, W. He, F. Pei, F. Wu, Y. Wu, J. Qian, Y. Cao, X. Ai, H. Yang, Synthesis and electrochemical behaviors of layered $Na_{0.67}Mn_{0.65}Co_{0.2}Ni_{0.15}O_2$ microflakes as a stable cathode material for sodium-ion batteries, J. Mater. Chem. A. 1 (2013) 3895–3899, https://doi.org/10.1039/C3TA01430D.

[34] X. Wang, M. Tamaru, M. Okubo, A. Yamada, Electrode properties of P2–Na $_{2/3}$ Mn $_y$ Co $_{1-y}$ O 2 as cathode materials for sodium-ion batteries, J. Phys. Chem. C. 117 (2013) 15545–15551, https://doi.org/10.1021/jp406433z.

[35] X. Chen, X. Zhou, M. Hu, J. Liang, D. Wu, J. Wei, Z. Zhou, Stable layered P3/P2 Na $_{0.66}$ Co $_{0.5}$ Mn $_{0.5}$ O $_2$ cathode materials for sodium-ion batteries, J. Mater. Chem. A. 3 (2015) 20708–20714, https://doi.org/10.1039/C5TA05205J.

[36] Q.-C. Wang, E. Hu, Y. Pan, N. Xiao, F. Hong, Z.-W. Fu, X.-J. Wu, S.-M. Bak, X.-Q. Yang, Y.-N. Zhou, Utilizing Co $^{2+}$/Co $^{3+}$ redox couple in P2-layered Na $_{0.66}$ Co $_{0.22}$ Mn $_{0.44}$ Ti $_{0.34}$ O $_2$ cathode for sodium-ion batteries, Adv. Sci. 11 (2017) 1700219, https://doi.org/10.1002/advs.201700219.

[37] A. Ponrouch, D. Monti, A. Boschin, B. Steen, P. Johansson, M.R. Palacín, Non-aqueous electrolytes for sodium-ion batteries, J. Mater. Chem. A. 3 (2015) 22–42, https://doi.org/10.1039/c4ta04428b.

[38] K. Vignarooban, R. Kushagra, A. Elango, P. Badami, B.E. Mellander, X. Xu, T.G. Tucker, C. Nam, A.M. Kannan, Current trends and future challenges of electrolytes for sodium-ion batteries, Int. J. Hydrogen Energy 41 (2016) 2829–2846, https://doi.org/10.1016/j.ijhydene.2015.12.090.

[39] X. Zheng, C. Bommier, W. Luo, L. Jiang, Y. Hao, Y. Huang, Sodium metal anodes for room-temperature sodium-ion batteries: Applications, challenges and solutions, Energy Storage Mater. 16 (2019) 6–23, https://doi.org/10.1016/j.ensm.2018.04.014.

[40] J.Y. Hwang, S.T. Myung, J.U. Choi, C.S. Yoon, H. Yashiro, Y.K. Sun, Resolving the degradation pathways of the O3-type layered oxide cathode surface through the nano-scale aluminum oxide coating for high-energy density sodium-ion batteries, J. Mater. Chem. A. 5 (2017) 23671–23680, https://doi.org/10.1039/c7ta08443a.

[41] H.V. Ramasamy, K. Kaliyappan, R. Thangavel, V. Aravindan, K. Kang, D.U. Kim, Y. Park, X. Sun, Y.-S. Lee, Cu-doped P2-Na $_{0.5}$ Ni $_{0.33}$ Mn $_{0.67}$ O $_2$ encapsulated with MgO as a novel high voltage cathode with enhanced Na-storage properties, J. Mater. Chem. A. 5 (2017) 8408–8415, https://doi.org/10.1039/C6TA10334K.

[42] Z. Jian, L. Zhao, H. Pan, Y.S. Hu, H. Li, W. Chen, L. Chen, Carbon coated $Na_3V_2(PO_4)_3$ as novel electrode material for sodium ion batteries, Electrochem. Commun. 14 (2012) 86–89, https://doi.org/10.1016/j.elecom.2011.11.009.

[43] (a) K. Kaliyappan, J. Liu, A. Lushington, R. Li, X. Sun, Highly Stable Na2/3 (Mn0.54Ni0.13Co0.13)O2 cathode modified by atomic layer deposition for sodium-ion Batteries, ChemSusChem 8 (2015) 2537–2543, https://doi.org/10.1002/cssc.201500155;
(b) T. Teranishi, Y. Yoshikawa, M. Yoneda, A. Kishimoto, J. Halpin, S.O. Brien, I. M. Povey, Aluminum interdiffusion into LiCoO2 using atomic layer deposition for high rate lithium ion batteries, ACS Appl. Energy Mater. 1 (2018) 3277–3282.

[44] Y. Liu, X. Fang, A. Zhang, C. Shen, Q. Liu, H.A. Enaya, C. Zhou, Layered P2-$Na_{2/3}[Ni_{1/3}Mn_{2/3}]O_2$ as high-voltage cathode for sodium-ion batteries: the capacity decay mechanism and Al_2O_3 surface modification, Nano Energy. 27 (2016) 27–34, https://doi.org/10.1016/j.nanoen.2016.06.026.

[45] J. Alvarado, C. Ma, S. Wang, K. Nguyen, M. Kodur, Y.S. Meng, Improvement of the cathode electrolyte interphase on P2-$Na_{2/3}Ni_{1/3}Mn_{2/3}O_2$ by atomic layer deposition, ACS Appl. Mater. Interf. 9 (2017) 26518–26530, https://doi.org/10.1021/acsami.7b05326.

[46] B. Ahmed, C. Xia, H.N. Alshareef, Electrode surface engineering by atomic layer deposition: A promising pathway toward better energy storage, Nano Today. 11 (2016) 250–271, https://doi.org/10.1016/j.nantod.2016.04.004.

[47] Y. Bai, X. Zhang, X. Wang, Z. Luo, G. Chen, Preparation and performances of novel Na_2FeSiO_4/C composite with more stable polymorph as cathode material of sodium-ion batteries, J. Power Sour. 430 (2019) 120–129, https://doi.org/10.1016/j.jpowsour.2019.05.015.

[48] P. Hou, F. Li, Y. Wang, J. Yin, X. Xu, Mitigating the P2–O2 phase transition of high-voltage P2-Na $_{2/3}$ [Ni $_{1/3}$ Mn $_{2/3}$]O $_2$ cathodes by cobalt gradient substitution for high-rate sodium-ion batteries, J. Mater. Chem. A. 7 (2019) 4705–4713, https://doi.org/10.1039/c8ta10980j.

[49] S. Amaresh, K. Karthikeyan, K.J. Kim, M.C. Kim, K.Y. Chung, B.W. Cho, Y.S. Lee, Facile synthesis of ZrO_2 coated Li_2CoPO_4F cathode materials for lithium secondary batteries with improved electrochemical properties, J. Power Sour. 244 (2013) 395–402, https://doi.org/10.1016/j.jpowsour.2012.12.010.

[50] K. Kaliyappan, J. Liu, A. Lushington, R. Li, X. Sun, Cathode modified by atomic layer deposition for sodium ion batteries by atomic layer deposition for sodium-ion batteries, ChemSusChem 3 (2015), https://doi.org/10.1002/cssc.201500155.

[51] L. Wang, Y.G. Sun, L.L. Hu, J.Y. Piao, J. Guo, A. Manthiram, J. Ma, A.M. Cao, Copper-substituted Na 0.67 Ni 0.3−x Cu x Mn 0.7 O 2 cathode materials for sodium-ion batteries with suppressed P2–O2 phase transition, J. Mater. Chem. A. 5 (2017) 8752–8761, https://doi.org/10.1039/C7TA00880E.

[52] J. Song, B. Xiao, Y. Lin, K. Xu, X. Li, Interphases in Sodium-Ion Batteries, Adv. Energy Mater. 8 (2018) 1–24, https://doi.org/10.1002/aenm.201703082.

[53] T. Risthaus, D. Zhou, X. Cao, X. He, B. Qiu, J. Wang, L. Zhang, Z. Liu, E. Paillard, G. Schumacher, M. Winter, J. Li, A high-capacity P2 Na $_{2/3}$ Ni $_{1/3}$ Mn $_{2/3}$ O 2 cathode material for sodium ion batteries with oxygen activity, J. Power Sour. 395 (2018) 16–24, https://doi.org/10.1016/j.jpowsour.2018.05.026.

[54] X. Wu, J. Guo, D. Wang, G. Zhong, M.J. McDonald, Y. Yang, P2-type $Na_{0.66}Ni_{0.33-x}Zn_xMn_{0.67}O_2$ as new high-voltage cathode materials for sodium-ion batteries, J. Power Sour. 281 (2015) 18–26, https://doi.org/10.1016/j.jpowsour.2014.12.083.

[55] S. Guo, Q. Li, P. Liu, M. Chen, H. Zhou, Environmentally stable interface of layered oxide cathodes for sodium-ion batteries, Nat. Commun. 8 (2017) 1–9, https://doi.org/10.1038/s41467-017-00157-8.

[56] S.C. Jung, H.J. Kim, J.W. Choi, Y.K. Han, Sodium ion diffusion in Al_2O_3: A distinct perspective compared with lithium ion diffusion, Nano Lett. 14 (2014) 6559–6563, https://doi.org/10.1021/nl503169v.

[57] K. Xu, Erratum: "charge-transfer" process at graphite/electrolyte interface and the solvation sheath structure of Li^+ in nonaqueous electrolytes, J. Electrochem. Soc. 154 (2007) S9, https://doi.org/10.1149/1.2536554.

[58] (a) Y. Wang, K. Tang, X. Li, R. Yu, X. Zhang, Y. Huang, G. Chen, S. Jamil, S. Cao, X. Xie, Z. Luo, X. Wang, Improved Cycle and Air Stability of P3-Na0.67Mn0.75Ni0.25O2 electrodes for Sodium-ion batteries Coated with Metal Phosphates, Chem. Eng. J. 372 (2019) 1066–1076, https://doi.org/10.1016/j.cej.2019.05.010;
(b) Y. Wang, X. Wang, X. Li, R. Yu, M. Chen, K. Tang, X. Zhang, The novel P3-type Na0.67Mn0.75Ni0.25O2 oxide doped by non-metallic elements for high performance sodium-ion batteries, Chem. Eng. J. 360 (2019) 139–147, https://doi.org/10.1016/j.cej.2018.11.214.

[59] S. Yuvaraj, S. Amaresh, Y.S. Lee, R.K. Selvan, Effect of carbon coating on the electrochemical properties of Co_2SnO_4 for negative electrodes in lithium ion batteries, RSC Adv. 4 (2014) 6407–6416.